Approach Based on Machine Learning for the Sensitivity Assessment of an Aerodynamic Shape

Hossein Jabbari[1] and Ali Esmaeili, Ph.D.[2]

Abstract: This study presents an innovative approach to the aerodynamic optimization of wing-in-ground (WIG) effect vehicles, with a focus on enhancing operational efficiency and promoting environmental sustainability. A coupled framework was developed in which Reynolds-averaged Navier–Stokes (RANS) computational-fluid-dynamics simulations were linked to an adaptive neuro-fuzzy inference system (ANFIS) surrogate, after which a genetic algorithm (GA) was employed for design exploration. Within this framework, the four-dimensional (4D) design space, defined by camber, thickness, angle of attack, and height-to-chord ratio (h/c), was traversed efficiently, and response-surface methodology was applied so that in-depth parameter sensitivities could be quantified. It was found that camber and ground clearance accounted for 36% and 31% of the variance in the lift-to-drag ratio, whereas angle of attack and thickness contributed 22% and 11%, respectively. By means of GA optimization guided by the ANFIS surrogate, a lift-to-drag (L/D) improvement of 55.9% over the baseline configuration was achieved. Numerical validation through three-dimensional (3D) WIG simulations confirmed that modifications to camber and ground clearance altered the velocity field in a manner consistent with induced-drag reduction, thereby substantiating the predicted performance gains. Owing to these enhancements, fuel consumption and associated emissions would be lowered, aligning the design with emerging environmental standards. These findings were shown to highlight the paramount importance of camber, ground clearance, angle of attack, and thickness in the aerodynamic sensitivity assessment and optimization of WIG vehicles, thereby affirming the capacity of machine learning–assisted approaches to revolutionize the practice of aerodynamic design. **DOI: 10.1061/JAEEEZ.ASENG-5804.**

Author keywords: Optimization; Machine learning; Sensitivity analysis; Aerodynamic shape; Ground effect.

Introduction

The next generation of commercial transport aerial vehicles will stand at a pivotal juncture, tasked with addressing environmental challenges and adhering to strict emissions targets by 2050 (Arnaldo Valdés et al. 2019). This has reignited interest in innovative design, especially in configurations that use the wing-in-ground effect to boost aerodynamic efficiency through ground proximity advantages (Jabbari et al. 2021; Yun et al. 2010). Achieving these designs requires progress in various engineering disciplines, including aerodynamics and structural design. Enhanced computational power and advances in numerical optimization have made computational fluid dynamics (CFD) simulations a key part of the design process, greatly aiding engineers in refining their designs (Koo and Zingg 2018).

Historically, the design optimization of wing-in-ground (WIG) vehicles, including wing sections and aerofoils near the ground, relied on CFD and genetic algorithms (GA). Despite their effectiveness, these methods faced challenges with the complex and variable nature of WIG design objectives, such as optimizing the lift-to-drag (L/D) ratio. Recent progress in aerodynamic shape optimization has been driven by the adoption of adjoint methods, introduced by pioneers like Pironneau (1974), Angrand (1983), and Jameson (1988). These methods efficiently compute the sensitivity of aerodynamic metrics, like lift and drag, to geometric modifications, aiding gradient-based optimization in achieving precise design goals. Unlike gradient-free methods, which falter in complex, high-dimensional scenarios, gradient-based approaches excel in reaching solutions efficiently in suitable design spaces (Simanowitsch et al. 2022; Zingg et al. 2008). Additionally, the advent of extensive parallel computing resources has enabled aerodynamicists to solve complex flow problems and apply demanding optimization algorithms, enhancing the breadth and depth of aerodynamic research and design.

Recent advancements in aerodynamic shape optimization (ASO) have been significantly enhanced by the integration of machine learning (ML) techniques, providing more efficient, scalable, and accurate methods to address complex aerodynamic challenges. In particular, the application of ML algorithms in optimizing the aerodynamic design of airfoils and wings has been pivotal in improving performance metrics such as the L/D ratio, a crucial determinant of aerodynamic efficiency.

Li et al. (2022) comprehensively reviewed the role of ML in ASO, emphasizing how it aids in reducing the dimensionality of design spaces, accelerating aerodynamic analysis, and enhancing optimization processes. The study highlighted the versatility of ML in dealing with large-scale design optimizations, particularly through methods such as physics-informed ML. The potential of these methods is seen in the reduction of training costs and the coupling of prior aerodynamic knowledge with machine learning models, an approach that promises to address scalability issues. Similarly, Hasan et al. (2025) developed a novel optimization framework that combines CFD with ML models, showcasing significant improvements in optimization efficiency. By using a surrogate model trained on a

[1]Graduate Researcher, Dept. of Mechanical Engineering, Engineering Faculty, Ferdowsi Univ. of Mashhad, Mashhad 91775-1111, Iran. Email: hossein.jabbari@mail.um.ac.ir

[2]Associate Professor, Dept. of Mechanical Engineering, Engineering Faculty, Ferdowsi Univ. of Mashhad, Mashhad 91775-1111, Iran (corresponding author). ORCID: https://orcid.org/0000-0002-5747-4341. Email: aliesmaeili@ferdowsi.um.ac.ir

Note. This manuscript was submitted on April 4, 2024; approved on May 19, 2025; published online on October 24, 2025. Discussion period open until March 24, 2026; separate discussions must be submitted for individual papers. This paper is part of the ***Journal of Aerospace Engineering***, © ASCE, ISSN 0893-1321.

large set of CFD simulations, the study achieved optimal aerodynamic configurations for transonic aircraft wings. This hybrid approach demonstrated a 14% improvement in L/D ratio, offering a cost-effective alternative to traditional CFD-based optimization.

Xu et al. (2021) further innovated the field by applying deep neural networks (DNNs) to predict adjoint vectors in ASO. The DNN-based approach reduced the computational cost of adjoint calculations while maintaining the accuracy of traditional adjoint methods. This is crucial for speeding up optimization processes without compromising the quality of results, particularly in high-fidelity simulations. Teimourian et al. (2024) explored a range of ML algorithms for predicting aerodynamic performance, including random forest and gradient boosting regression. Their findings revealed that random forest outperformed other methods in predicting L/D ratios, with significant reductions in both training and evaluation times, offering a highly efficient method for real-time optimization. In addition, Lou et al. (2023) demonstrated the use of deep reinforcement learning (DRL) for airfoil optimization, where a combination of DNNs and a double deep Q-network (DQN) optimized the airfoil's L/D ratio. This approach proved particularly effective in handling the nonlinearity of aerodynamic performance, achieving a 71.46% improvement in the L/D ratio. The integration of DRL in optimization processes highlights its potential to autonomously explore design spaces and adapt to varying computational conditions.

The integration of machine learning and optimization techniques marks a transformative shift in the field of aerodynamic design. These methodologies not only accelerate the design process but also allow for more precise and scalable solutions that are increasingly necessary for complex systems like WIG vehicles. The collective contribution of these studies sets the stage for the development of more robust, sustainable, and efficient aerodynamic designs, thereby advancing the broader goals of optimizing energy consumption and reducing environmental impact in aerospace engineering.

During aerodynamic shape operations close to the ground, the wingtip vortices are constrained by the proximity to the surface, limiting their vertical expansion. This restriction causes the vortices to stretch horizontally along the ground, effectively elongating the wake's spanwise dimension. Such a phenomenon results in an augmented effective aspect ratio for the wing, mimicking the effect of a longer wingspan. This adjustment leads to a decrease in induced drag, thereby enhancing the aerodynamic performance as evidenced by an improved L/D ratio. Additionally, the ground effect alters the airflow dynamics around the wing, shifting the stagnation point to the wing's lower surface. This shift redirects a substantial amount of the oncoming air to flow over the top surface of the wing (Ahmed et al. 2007). Consequently, the velocity of air under the wing diminishes, resulting in a heightened air pressure that creates a supportive air cushion effect. In the context of WIG, designed for low-altitude flight, this air cushion leads to an additional lift contribution due to RAM pressure (the dynamic pressure resulting from flow stagnation, $q = 1/2\ \rho U^2$) (Jesudasan et al. 2023). This force significantly enhances the aerodynamic shape's overall performance, allowing for heavier payloads or extended range on the same amount of fuel when compared to conventional aerial vehicles operating at higher altitudes.

A major challenge in WIG design and operation is the effect of wind gusts on pitch angle and altitude, necessitating systems that allow WIG crafts to autonomously return to their original positions without pilot intervention. The critical role of lift coefficient variation with flight altitude is essential for maintaining WIG's static height stability. Adjusting the center of gravity alone is insufficient for ensuring altitude stability (Jesudasan et al. 2023). Fevralskikh (2022), recently proposed a method using RANS-based simulations to analyze longitudinal static height stability for WIG aircraft under cruising conditions.

Aerodynamic optimization has evolved from simple, inviscid two-dimensional scenarios to more complex, three-dimensional problems, thanks to advancements in technology and algorithms. Early work by pioneers like Jameson and Reuther (1994), applied the continuous adjoint approach with Euler equations to improve aerofoil designs on structured grids. This was followed by the integration of turbulence models by researchers such as Anderson and Bonhaus (1999) and Nemec et al. (2004), further advancing aerofoil optimization. The shift toward three-dimensional (3D) optimization saw significant contributions like Elliot and Peraire's application (Elliott and Peraire 1997) of the Euler equations and Nielsen and Anderson's adaptation (Nielsen and Anderson 1999) of the Spalart–Allmaras turbulence model on unstructured grids. Research focusing on aerofoil design optimization aimed at enhancing aerodynamic performance and static stability (Hu et al. 2022; Lee and Lee 2013; Park and Lee 2010), especially for WIG applications, highlighted the beneficial impact of S-shaped camber lines on lift-induced ground effect factors, crucial for improving stability and efficiency near the ground. While initial efforts concentrated on refining wing shapes for better performance, the pressing need to reduce carbon emissions in aviation demands more versatile solutions. Such solutions should support broader design considerations, aiding engineers in early design decisions through comprehensive analyses. This approach paves the way for optimizing and assessing innovative designs, including blended wing-body, box wing, strut-braced wings, and double-bubble configurations, aligning with the industry's sustainability goals (Gagnon and Zingg 2016; Koo and Zingg 2018; Reist and Zingg 2017).

From approximately 2005–2025, there has been significant advancement in high-fidelity, gradient-based aerodynamic optimization, mainly benefiting the detailed design phase of nearly optimal solutions (Koo and Zingg 2018; Lyu and Martins 2014; Morris et al. 2009). However, the focus has recently shifted toward creating rapid, low-fidelity simulation tools for the aerodynamic shape optimization of wings. Researchers like Jansen et al. (2010), have explored panel methods for induced drag assessment and viscous drag predictions on nonplanar surfaces. Similarly, studies by Ning and Kroo (2010), and Conlan-Smith et al. (2020), have investigated winglets and optimized wing planforms using vortex-lattice and panel methods, respectively, to minimize induced drag, incorporating tools like XFOIL (an interactive airfoil analysis and design code for subsonic airfoils that couples panel methods with a viscous/inviscid boundary_layer model) for enhanced viscous drag analysis (Conlan-Smith et al. 2022). Abu Salem et al. (2023), introduced a vortex lattice method to consider aerodynamics during ground effect, crucial for conceptualizing take-off phases of box-wing plane. This approach, beneficial for early design stages, allows for the integration of multiple objectives, including stability considerations. By employing gradient-free optimizers, it enables a holistic exploration of design possibilities, merging aerodynamic efficiency with longitudinal stability in WIG vehicles, offering valuable insights for preliminary design phases, particularly when design databases are limited (Jesudasan et al. 2023). In the dynamic field of design, the importance of multimodality, or the existence of multiple optimal solutions, is increasingly recognized. Gradient-based methods quickly converge to an optimal solution but may fall into local minima. In contrast, stochastic methods can find global optima but slow down as the number of design variables grows (Aly et al. 1996; Zingg et al. 2008). Chernukhin and Zingg's (2013) research demonstrates that a gradient-based multistart method can efficiently navigate multimodality to achieve global optimization, underscoring its utility in complex design environments.

This study emphasizes optimizing the aerofoil shape, ground clearance (h/c), angle of attack (AOA), thickness (t), and camber (Ca) of WIG vehicles, crucial for their aerodynamic performance and operational efficiency. It explores the ground effect, which significantly alters aerodynamic forces when a wing is near a surface, using ANFIS to navigate the complex, noisy objective function for a more efficient optimization process. The novelty lies in its methodological approach and detailed sensitivity analysis, investigating how key design variables affect WIG vehicles' aerodynamic performance to find optimal configurations that maximize the ground effect. This study addresses the longstanding gap in WIG vehicle optimization by introducing a machine learning component, specifically ANFIS, into the established GA–CFD framework. Previous research primarily focused on GAs and CFD without leveraging data-driven surrogates to manage the complex, multi-dimensional design space. By integrating ANFIS, the predictive accuracy and computational efficiency have been enhanced, enabling the optimization process to converge more rapidly on high L/D ratios under near-ground conditions. This approach not only refines the aerodynamic design of WIG vehicles but also advances the broader field of aerodynamic optimization by illustrating how machine learning can be employed to augment and streamline traditional methods.

Methodology

A custom MATLAB code was developed to interface with Gambit and Fluent for geometry creation, mesh generation, and the numerical solution of the governing equations. This framework allowed for a smooth progression from parameterization to final analysis, ensuring that the optimization process was both efficient and comprehensive. The overall approach consisted of five interconnected stages: (1) parameterization and geometric control, (2) structured mesh generation, (3) solution of the flow equations via the finite volume method, (4) evaluation of gradients and sensitivities, and (5) use of an optimization algorithm. The GA was employed to explore a broad design space for WIG vehicles, while an ANFIS provided a predictive model for intermediate aerodynamic outputs.

Geometry Parameterization, Control, and Mesh Manipulation

Numerical simulations were performed on a structured mesh, selected for its suitability in capturing flow features near the ground, where rapid changes in velocity and pressure occur. Fig. 1 illustrates the design of these two-dimensional (2D) structured grids. A computational mesh with an H-shaped topology was constructed around the full-span wing using quadrilateral elements. These elements were specifically refined in areas requiring higher resolution, with grid size restrictions and other attributes tailored to align with experimental conditions. To ensure that boundary effects were minimized, the computational domain was sufficiently expanded. An open boundary condition, defined as a pressure outlet, was applied at the outflow boundary to simulate an open-system environment. No-slip boundary conditions were imposed at all solid surfaces, while the other boundaries of the domain were designated as far-field boundaries. The top and front boundaries were positioned at a distance of 10 times the aerofoil chord length, while the downstream boundary was placed 30 times the chord length away from the aerofoil's leading edge, as illustrated in Fig. 1(a). Given that the lower boundary of the computational domain corresponds to the ground surface, a boundary layer forms near this surface. Consequently, the atmospheric velocity profile is incorporated into the simulation to capture the realistic flow dynamics near the ground. As highlighted in Djavareshkian et al. (2011), a study on domain independence was performed, and the final domain configuration was chosen after testing various lengths for the upstream, downstream, and top boundaries. The final dimensions of the domain were selected to match the configurations used by previous studies (Li et al. 2017; Foshat 2020).

The velocity profile is derived from the solution of the Blasius equation, which provides the boundary layer thickness at the inlet. This inlet profile accounts for the velocity components, where the vertical component $v(y)$ is much smaller than the streamwise component $u(y)$. However, the relationship between these components must be considered to avoid artificial effects in the pressure field near the inlet. For this simulation, the inlet boundary conditions

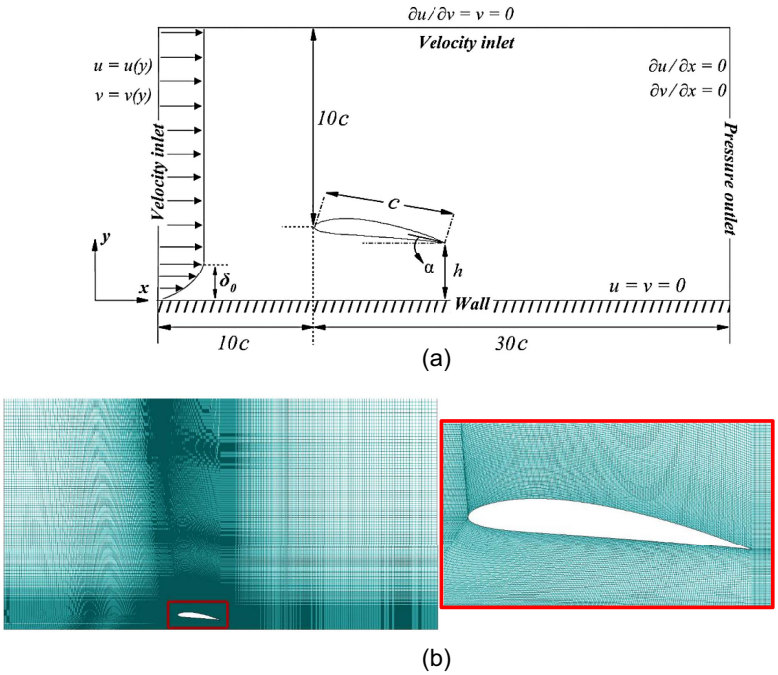

Fig. 1. (a) Dimension and boundary condition of 2D domain; and (b) H-grid topology and zoom-out and zoom-in H grid.

included a velocity distribution with a boundary layer thickness of $\delta_0 = 0.41c$ at $Re = 2.4 \times 10^5$. As the flow reaches the aerofoil, the boundary layer thickness increases to $\delta = 1.0c$, corresponding to $Re_x = 2.3 \times 10^{11}$ at the aerofoil section.

The computational aerofoil was allowed to move perpendicularly to the ground surface, maintaining the boundary layer thickness of $\delta = 1.0c$ at the leading edge of the aerofoil. To prevent computational errors such as inverted cell volumes and high mesh skewness, the distance between the first cell near the solid walls was kept to a minimum. This also ensured that the maximum value of the wall-normal length in wall units was close to unity. Finally, the impact of meshing density around the infinite wing was analyzed. The optimum number of cells was determined to ensure that the results were independent of the mesh, thereby guaranteeing the accuracy and robustness of the numerical simulations.

In this study, a standard $k-\varepsilon$ turbulence model with standard wall functions was employed to capture the boundary layer behavior near the aerofoil and ground surfaces. The computational mesh was designed so that the first cell adjacent to the walls maintained y^+ values within the recommended range for standard wall-function treatments, typically between 30 and 100. This choice prevented the need for fully resolving the viscous sublayer and allowed the boundary-layer profile to be modeled accurately within the constraints of the standard wall-function approach. Because the standard $k-\varepsilon$ turbulence model relies on wall functions to approximate flow behavior in the near-wall region, the numerical setup was configured accordingly. By ensuring that y^+ remained in the target window, the wall functions could provide stable and reliable results for the flow conditions of this WIG vehicle optimization problem. This approach reduced computational expense while retaining the fidelity needed to evaluate lift and drag across the design space. Consequently, the study did not employ a low Reynolds-number formulation or enhanced wall treatment, as the selected turbulence model and the mesh resolution were sufficient for the operational Reynolds numbers considered here.

Grid independence was confirmed by refining the mesh until further increases in grid resolution did not produce significant changes in aerodynamic outputs, specifically the pressure coefficient (C_p) and skin friction coefficient (C_f). Fig. 2 presents an example of the grid refinement study, demonstrating that the distribution of C_p and C_f converged as the mesh density increased. To ensure the numerical accuracy and reliability of the computed aerodynamic coefficients, a rigorous mesh independence analysis was performed. Four mesh configurations, ranging from 11×10^4 to 13.58×10^4 elements, were assessed at a $Re = 2.4 \times 10^5$, $AOA = 10°$, and $h/c = 0.2$ for the NACA 0015 aerofoil. Figs. 2(a and b) illustrate the C_p and C_f distributions over the aerofoil surfaces were compared across these mesh densities. Results clearly indicate that the variations in both C_p and C_f distributions are negligible between the two finest meshes (13×10^4 and 13.58×10^4 elements). The mesh comprising 13×10^4 elements was selected for subsequent simulations, providing an optimal balance between computational cost and accuracy. The mesh was progressively refined, and the corresponding lift and drag coefficients were monitored until further refinement produced negligible changes. Fig. 2 illustrates the aerodynamic coefficients converge based on the dimensionless time $(time \times U_\infty/c)$ beyond a specific mesh density, thereby confirming that the final mesh resolution accurately captures the flow features pertinent to

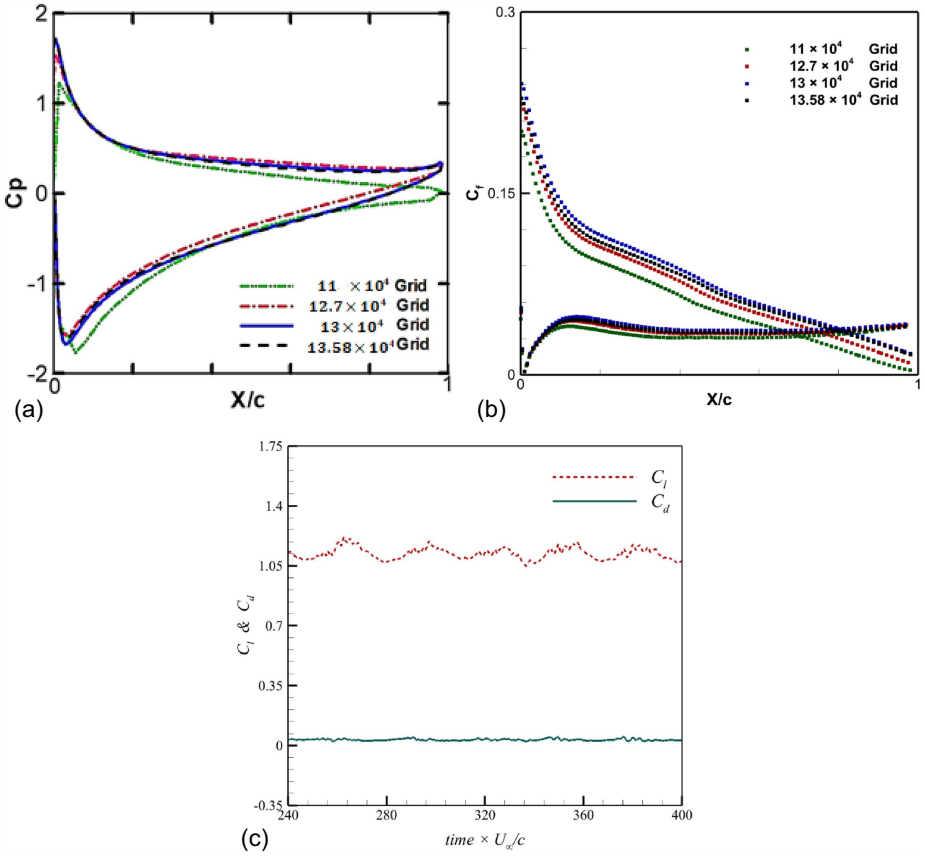

Fig. 2. (a) Effect of grid sizing on surface pressure coefficient c_p; (b) effect of grid sizing on skin-friction coefficient c_f; and (c) time histories of lift and drag coefficients, c_l and c_d, indicating convergence for α = 10° and $h/c = 0.2$.

Table 1. Settings for numerical simulation

CFD attribute	Computational configuration
Flow	turbulent
Solver	2D double precision
Momentum equation solver	Normalize variable diagram
Solver	SIMPLE
turbulent model	$k-\varepsilon$ standard wall functions
Bounded scheme	Scaled boundary integral condition (SBIC)

this investigation. This convergence analysis ensures confidence in the fidelity of the aerodynamic coefficients reported in the subsequent sections.

This approach was repeated for domain size independence by examining multiple backward, forward and up dimensions, with the final selection dictated by negligible differences in aerodynamic results. Table 1 summarizes the simulation parameters, including the Reynolds number, which was set at 2.4×10^5. The flow boundary conditions were selected to mirror near ground operation for WIG vehicles.

A validation of the numerical model was carried out by comparing the computed surface pressure on a NACA 0015 aerofoil to experimental data (Ahmed and Sharma 2005). The close agreement, shown in Fig. 3, confirms that the grid resolution and domain extent were sufficient to capture the essential flow physics.

ANFIS Model Training and Data Preparation

The ANFIS was employed to approximate the aerodynamic performance for various design configurations. The ANFIS model incorporated a Sugeno-type fuzzy inference system with rules of the form:

$$\begin{aligned} &Rule\ 1\text{: if } x \text{ is } A_1 \text{ and } y \text{ is } B_1, \quad z_1 = p_1x + q_1y + r_1 \\ &Rule\ 2\text{: if } x \text{ is } A_2 \text{ and } y \text{ is } B_2, \quad z_2 = p_2x + q_2y + r_2 \end{aligned} \tag{1}$$

where x and y = design inputs (for instance, camber and angle of attack); A_i and B_i = fuzzy sets; and p_i, q_i, r_i = linear (consequent) parameters. The membership functions μ_{A_i} and μ_{B_i} were selected as Gaussian functions

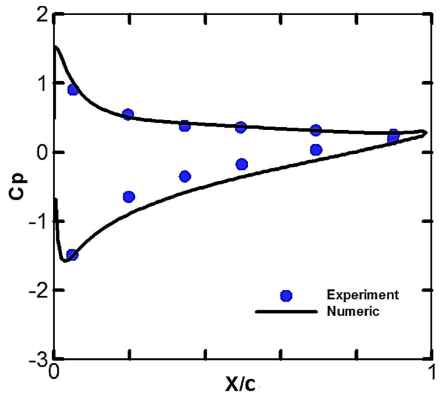

Fig. 3. Comparison pressure coefficient distribution of present numerical result with experimental data for aerofoil NACA 0015 for an AOA 10° and $h/c = 0.2$.

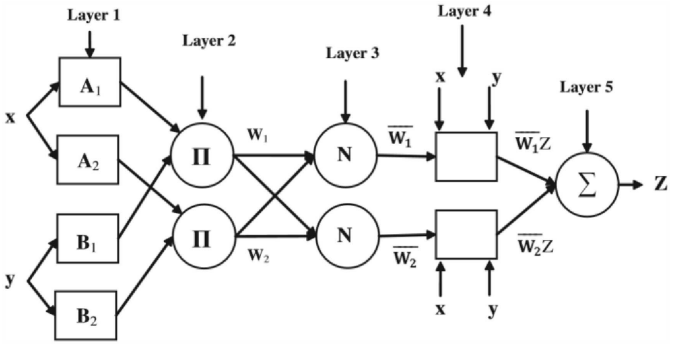

Fig. 4. ANFIS architecture. (Reprinted from *Ocean Engineering*, Vol. 59, M. Chiarello and R. Zinno, "Neuro-fuzzy based approach for estimation of Hydrofoil performance," pp. 1–8, © 2013, with permission from Elsevier.)

$$\mu_{A_i}(x) = \exp\left[-\frac{(x-c)^2}{2\sigma^2}\right] \tag{2}$$

where c = center; and σ = width of the membership function. The training involved five layers, as depicted in Fig. 4 of the theoretical routines. Further details regarding this method, including the relevant equations and parameters, can be found in Djavareshkian and Esmaeili (2013).

The overall workflow of the ANFIS approach is summarized in Fig. 5. The ANFIS system comprises five layers, each performing specific functions:

- **Layer 1**: Each node in this layer is associated with an input variable (e.g., camber or angle of attack) and computes a membership function to represent the degree of membership for each fuzzy set. The membership function can be defined as Gaussian, where based on Eq. (2), μ_{A_i} and μ_{B_i} are the Gaussian membership functions for inputs x and y:

$$O_1^1 = \mu_A(x), \qquad O_2^1 = \mu_B(y) \tag{3}$$

- **Layer 2**: The nodes in this layer compute the firing strength of each rule by multiplying the incoming signals from Layer 1. This gives us the rule strength

$$O_1^2 = \omega_1 = \mu_A(x) \cdot \mu_B(y), \qquad O_2^2 = \omega_2 = \mu_A(x) \cdot \mu_B(y) \tag{4}$$

- **Layer 3**: Normalization of the firing strengths takes place here, which ensures that the sum of all rule strengths is equal to 1

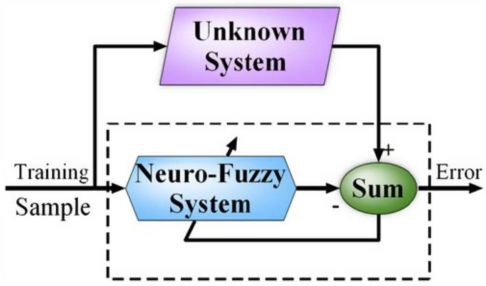

Fig. 5. Process of ANFIS. (Reprinted from *Ocean Engineering*, Vol. 59, M. Chiarello and R. Zinno, "Neuro-fuzzy based approach for estimation of Hydrofoil performance," pp. 1–8, © 2013, with permission from Elsevier.)

$$O_1^3 = \frac{\omega_1}{\omega_1 + \omega_2}, \qquad O_2^3 = \frac{\omega_2}{\omega_1 + \omega_2} \tag{5}$$

- **Layer 4**: In this layer, the consequent parameters p_i, q_i, r_i are adjusted based on the firing strengths calculated in Layer 3. The output of each node is calculated as

$$O_1^4 = \omega_1 \cdot (p_1 x + q_1 y + r_1), \qquad O_2^4 = \omega_2 \cdot (p_2 x + q_2 y + r_2) \tag{6}$$

- **Layer 5**: The final output is calculated by summing the outputs from Layer 4, weighted by their respective ring strengths

$$O^5 = \sum_{i=1}^{2} \omega_i z_i = \frac{\omega_1 z_1 + \omega_2 z_2}{\omega_1 + \omega_2} \tag{7}$$

In this study, the ANFIS model was trained to approximate aerodynamic coefficients (e.g., lift and drag) for each combination of design variables. These variables included camber, thickness, angle of attack, and ground clearance, all systematically varied within their prescribed ranges. Each sampled configuration was evaluated through CFD, yielding a database of input output pairs. The raw data were then screened for numerical anomalies (such as diverging flow solutions) and scaled to a uniform range to avoid bias arising from differences in parameter magnitudes.

The training process followed a hybrid strategy, combining the least squares (LS) method and the backpropagation (BP) algorithm (Jang et al. 1997). During the forward pass, the premise parameters (the centers and widths of the membership functions) were held fixed, allowing the LS solver to estimate the consequent parameters (p_i, q_i, r_i). In the backward pass, the BP algorithm updated the premise parameters based on the error signals propagated from the output. These errors were quantified using standard performance metrics such as mean squared error (MSE), normalized mean squared error (NMSE), mean absolute error (MAE), and the coefficient of determination R^2. The goal was to minimize MSE and NMSE and to maximize R^2, indicating a close match between ANFIS predictions and CFD derived references

$$\text{MSE} = \frac{1}{N} \sum_{i=1}^{N} (O_i + T_i)^2 \tag{8}$$

$$\text{NMSE} = \frac{1}{\sigma^2} \cdot \frac{1}{N} \sum_{i=1}^{N} (O_i + T_i)^2 \tag{9}$$

$$R^2 = 1 - \frac{\sum_{i=1}^{N} (O_i + T_i)^2}{\sum_{i=1}^{N} (O_i + \overline{T})^2} \tag{10}$$

where O_i = predicted aerodynamic coefficient; T_i = CFD (target) aerodynamic coefficient; σ^2 = variance of the target data; and $\overline{T}$ = mean of T_i. Convergence was deemed satisfactory when incremental reductions in MSE and NMSE became negligible and R^2 approached unity.

By consolidating the CFD results into this trained ANFIS model, new aerodynamic predictions could be obtained without running additional CFD simulations. In subsequent steps, the GA leveraged these rapid ANFIS evaluations to locate promising regions of the design space. This process allowed for a more efficient search for optimal L/D ratios, substantially reducing computational cost while maintaining a high level of accuracy in aerodynamic assessments.

Results and Discussion

In this study, the effects of aerofoil camber and thickness on aerodynamic performance near the ground were systematically explored using numerical simulations. The primary focus was on their impact on key aerodynamic coefficients, including C_l, C_d, and L/D ratio. These parameters were analyzed under varying conditions of angle of attack and ground clearance, which are critical for the efficient design of WIG effect vehicles.

Initial simulations considered three distinct angles of attack: 2.5°, 5°, and 7.5° and three different ground clearances, categorized as $h/c = 0.1$, 0.5, and 0.8. This variation enabled a comprehensive study of how these factors influence the performance of the aerofoil under different operational conditions, especially near the ground. The camber and thickness of the aerofoil were varied systematically, with camber values ranging from 0 to 0.04, and thickness values from 0.09 to 0.15 (nondimensional). This enabled a detailed analysis of the interaction between these parameters and their effects on aerodynamic efficiency. The study evaluated the aerodynamic performance of five distinct 2D aerofoils, each chosen for its varied camber and thickness configurations. The results, presented in Tables 2–6, illustrate how C_l and C_d evolve with changes in both angle of attack and ground clearance.

From the data in Tables 2–6, it is observed several significant trends that highlight the effects of ground clearance and camber on aerodynamic performance. For all configurations, as the aerofoils moved closer to the ground (decreasing h/c), there was a consistent increase in the lift coefficient. This outcome can be attributed to the ground effect, which effectively reduces the downwash and accelerates the airflow beneath the wing, increasing the pressure differential between the top and bottom surfaces (Jabbari et al. 2021). These changes result in an enhanced lift generation, particularly noticeable at higher angles of attack.

The increase in camber significantly enhances the lift coefficient, as evidenced in Tables 5 and 6. For instance, at a constant angle of attack and ground clearance, a camber value of 0.04 (as seen in Table 6) shows a marked improvement in lift at all ground clearance levels, compared to the baseline case with zero camber (Table 2). This aligns with theoretical expectations, as increasing camber increases the curvature of the mean aerodynamic chord, leading to higher lift at a given angle of attack (Chang 1970; Gudmundsson 2022). Interestingly, the effect of increasing thickness on lift is more nuanced. While an increase in thickness from 0.09 to 0.12 (Tables 2 and 3) results in a moderate increase in lift at

Table 2. Lift and drag coefficients of the mentioned aerofoils, $t/c = 0.09$, $Ca/c = 0$

	h/c								
	0.1			0.5			0.8		
AOA (degrees)	C_l	C_d	L/D_{num}	C_l	C_d	L/D_{num}	C_l	C_d	L/D_{num}
2.5	0.322	0.0123	26.18	0.312	0.0130	24	0.298	0.0142	20.98
5	0.680	0.0192	35.41	0.556	0.0222	25.04	0.539	0.0224	24.06
7.5	0.890	0.0398	22.36	0.775	0.0390	19.87	0.753	0.0405	18.59

Table 3. Lift and drag coefficients of the mentioned aerofoils, $t/c = 0.12$, $Ca/c = 0$

	h/c								
	0.1			0.5			0.8		
AOA (degrees)	C_l	C_d	L/D_{num}	C_l	C_d	L/D_{num}	C_l	C_d	L/D_{num}
2.5	0.315	0.0140	22.5	0.308	0.0175	17.6	0.295	0.0180	16.38
5	0.645	0.0220	29.31	0.555	0.0230	24.13	0.535	0.0256	20.89
7.5	0.860	0.0350	24.57	0.765	0.0380	20.13	0.743	0.0395	18.81

Table 4. Lift and drag coefficients of the mentioned aerofoils, $t/c = 0.15$, $Ca/c = 0$

	h/c								
	0.1			0.5			0.8		
AOA (degrees)	C_l	C_d	L/D_{num}	C_l	C_d	L/D_{num}	C_l	C_d	L/D_{num}
2.5	0.370	0.0178	20.78	0.275	0.0220	12.5	0.265	0.0230	11.52
5	0.600	0.0230	26.08	0.550	0.0235	23.40	0.520	0.0290	17.93
7.5	0.803	0.0335	23.97	0.740	0.0340	21.76	0.730	0.0380	19.21

Table 5. Lift and drag coefficients of the mentioned aerofoils, $t/c = 0.15$, $Ca/c = 0.02$

	h/c								
	0.1			0.5			0.8		
AOA (degrees)	C_l	C_d	L/D_{num}	C_l	C_d	L/D_{num}	C_l	C_d	L/D_{num}
2.5	0.545	0.0182	29.94	0.446	0.0265	16.83	0.429	0.0280	15.32
5	0.777	0.0271	28.67	0.683	0.0289	22.91	0.661	0.0324	20.40
7.5	0.987	0.0353	27.96	0.890	0.0402	22.14	0.880	0.0450	19.55

Table 6. Lift and drag coefficients of the mentioned aerofoils, $t/c = 0.15$, $Ca/c = 0.04$

	h/c								
	0.1			0.5			0.8		
AOA (degrees)	C_l	C_d	L/D_{num}	C_l	C_d	L/D_{num}	C_l	C_d	L/D_{num}
2.5	0.710	0.0280	25.35	0.665	0.0285	23.33	0.636	0.0295	21.56
5	0.970	0.0340	28.52	0.860	0.0350	24.57	0.825	0.0360	22.92
7.5	1.110	0.0450	24.66	1.051	0.0470	22.36	1.017	0.0500	20.34

$h/c = 0.1$ and 0.5, the impact diminishes at higher thickness values (Table 4; $t/c = 0.15$). This suggests that beyond a certain point, additional thickness has diminishing returns on lift generation. This behavior can be explained by the relationship between thickness and the boundary layer development. A thicker aerofoil delays boundary layer separation, but it also induces higher drag.

As expected, the drag coefficient exhibits a strong dependence on angle of attack, especially at higher values of AOA. For the slender aerofoils ($t/c = 0.09$), Table 2 shows that drag initially decreases as the angle of attack increases from 2.5° to 5°. However, at angles of attack beyond 5°, drag increases significantly, particularly for configurations with higher camber and thicker aerofoils. This trend is consistent with aerodynamics theory, which indicates that as the angle of attack increases, the flow over the aerofoil accelerates and starts to separate, increasing pressure drag. The observed increase in drag with AOA for aerofoils with larger camber (Tables 5 and 6) further supports this understanding. These aerofoils, while generating greater lift, also experience more pronounced adverse pressure gradients, leading to higher drag, especially at higher AOAs. This emphasizes the trade-off between lift and drag, which is a critical factor in the optimization of WIG vehicles. It is observed that ground clearance significantly affects both lift and drag (Zhang and Zerihan 2003).

The L/D ratio is a critical performance indicator in aerofoil design because it determines the aerodynamic efficiency of the vehicle. In this study, the L/D ratio was maximized by optimizing camber, thickness, and angle of attack. For the configurations with a camber of 0.04 (Table 6), L/D ratios were consistently higher than those with lower camber values, particularly at $h/c = 0.1$ and 0.5. This result underscores the importance of camber in optimizing lift without a disproportionate increase in drag. Additionally, the L/D ratio analysis reveals a significant improvement in efficiency as the angle of attack increases from 2.5° to 5°, but beyond this point, efficiency declines as the drag becomes dominant. The most efficient configurations, with the highest L/D ratios, were achieved at moderate angles of attack (around 5°) and ground clearances of approximately $h/c = 0.21$, as indicated in the final optimization phase (see Table 7).

Achieving higher L/D ratios is not only fundamental to improving the aerodynamic efficiency of WIG vehicles but also plays a

Table 7. Optimum evolution through the optimization process

Iteration	Ca/c	t/c	h/c	AOA	L/D (Num)	L/D (Exp)	Error
1	0.027231	0.090668	0.15849	5.599149	50.86131	78.4976	0.5434
2	0.036374	0.128617	0.100028	4.590905	48.27466	58.96697	0.2215
3	0.006776	0.121175	0.441397	6.514787	38.5398	89.4662	1.3214
4	0.01394	0.149609	0.310155	6.765366	44.71955	499.6074	10.1720
5	0.039972	0.09182	0.463464	2.506357	47.16021	103.304	1.1905
6	0.021215	0.117564	0.461439	6.812015	45.49118	118.6663	1.6086
7	0.032887	0.110406	0.30871	7.499979	48.74628	112.7825	1.3137
8	0.039851	0.1489	0.674642	5.925432	42.10934	182.255	3.3281
9	0.039999	0.121178	0.407163	5.989271	45.43105	128.1866	1.8216
10	0.039954	0.130252	0.103006	6.889729	53.08276	64.26528	0.2107
11	0.039964	0.090197	0.12102	6.518227	50.37813	90.54703	0.7973
12	0.000195	0.090106	0.75419	5.822818	26.0496	203.5427	6.8137
13	0.03362	0.123377	0.239996	6.962016	53.43064	80.35744	0.5040
14	0.036378	0.095877	0.10014	4.559088	18.70337	71.07249	2.8000
15	0.039997	0.100279	0.305443	2.500057	49.08034	96.46776	0.9655
16	0.039819	0.101607	0.487226	3.664517	49.4828	123.8444	1.5028
17	0.025695	0.128252	0.103369	6.419321	50.92223	61.43198	0.2064
18	0.039919	0.121677	0.212234	6.678779	55.88702	58.60953	0.0487

crucial role in enhancing their economic viability. The L/D ratio directly influences operational fuel efficiency and range, making it a key parameter in the optimization of aerofoil configurations. As such, this study investigates the impact of four essential design parameters, camber, thickness, angle of attack, and h/c ratio, on the L/D ratio, aiming to identify the optimal aerodynamic configuration under different operational conditions. In this context, GA are employed to facilitate the optimization process. GA provides a powerful search methodology, enabling the exploration of complex and high-dimensional design spaces by mimicking the natural process of selection and evolution. By leveraging GA, numerical simulations can efficiently explore the relationships between the aforementioned parameters and the L/D ratio, identifying configurations that maximize aerodynamic performance.

To achieve this, the study makes use of the data presented in Tables 2–6, which outlines the variation of lift and drag coefficients with changes in angle of attack and ground clearance. These values serve as the basis for constructing preliminary search domains, focusing on optimizing aerodynamic coefficients (C_l and C_d) under various design parameters. The use of such data ensures a rigorous exploration of the parameter space, providing a foundation for defining the regions of interest in the optimization process. The integration of ANFIS enhances the optimization approach by introducing a robust, data-driven framework for modeling complex nonlinear relationships between the input parameters and the aerodynamic performance. ANFIS, which combines the strengths of both fuzzy logic and artificial neural networks, is used to develop rules that precisely define the search areas within the design space. Here the ANFIS model represents the nonlinear relationship between the input parameters and the output (L/D ratio) through a series of weighted sums of linear functions:

$$f(x,y) = (\nu_1 x)p_1 + (\nu_1 y)q_1 + (\nu_1)r_1 + (\nu_2 x)p_2 + (\nu_2 y)q_2 + (\nu_2)r_2 \tag{11}$$

where ν_i = normalized ring strengths; and p_i, q_i, r_i $(i = 1, 2)$ = design parameters.

The architecture of ANFIS encompasses four distinct layers, incorporating two types of modifiable parameters: premise and consequent. Throughout the training phase, the system fine-tunes these parameters, specifically, the premise parameters within the initial layer and the consequent parameters in the terminal fourth layer, to ensure the fuzzy inference system (FIS) operates as intended. This study employs a hybrid learning strategy that merges the efficiency of the LS method with the dynamic adaptability of the BP algorithm, facilitating swift and effective FIS training. Once the premise parameters of the membership functions are established, the ANFIS's output is determined through a linear combination of the consequent parameters, ensuring a precise and responsive adaptation process.

Nevertheless, an approximation of the optimal L/D value (η_{app}) is obtained using the active set method, which finds the global maximizer of the constructed surfaces. For the design parameters (*i.e.*, t/c, Ca/c, h/c, and AOA) yielding η_{app}, an additional numerical simulation is conducted to get η_{num}, which is compared to η_{app}. The convergence criterion in Eq. (12) decides if a new searching space is needed or not:

$$\varepsilon = \left| \frac{\eta_{num} - \eta_{app}}{\eta_{app}} \right| < 5\% \tag{12}$$

When a new space becomes necessary, the region of interest is methodically reduced, and further experiments are conducted surrounding the most recently identified point to assess η_{app} (see Fig. 6).

In this research, the development of 18 unique search domains marked the progression toward achieving optimization. Illustrated in Fig. 7, these domains were finalized at the ultimate stage of optimization, showcasing a defined area of interest. Additionally, the key numerical findings from the optimization journey are detailed in Table 7. The optimal set of design parameters, achieving the highest efficiency (η), was identified as the objective of this study.

The subsequent analysis revealed the ideal characteristics for the aerodynamic profile of both the moving aerofoil under dynamic conditions and the aerofoil in a static state, derived through GA techniques. The findings, detailed in Table 7, indicate that the most efficient moving aerofoil configuration boasts a camber of 3.99% and a thickness of 12.17%. Furthermore, the analysis determined that the optimal wing section should maintain a proximity of approximately 0.21 to the ground, with the most effective angle of attack slightly exceeding 6.68°.

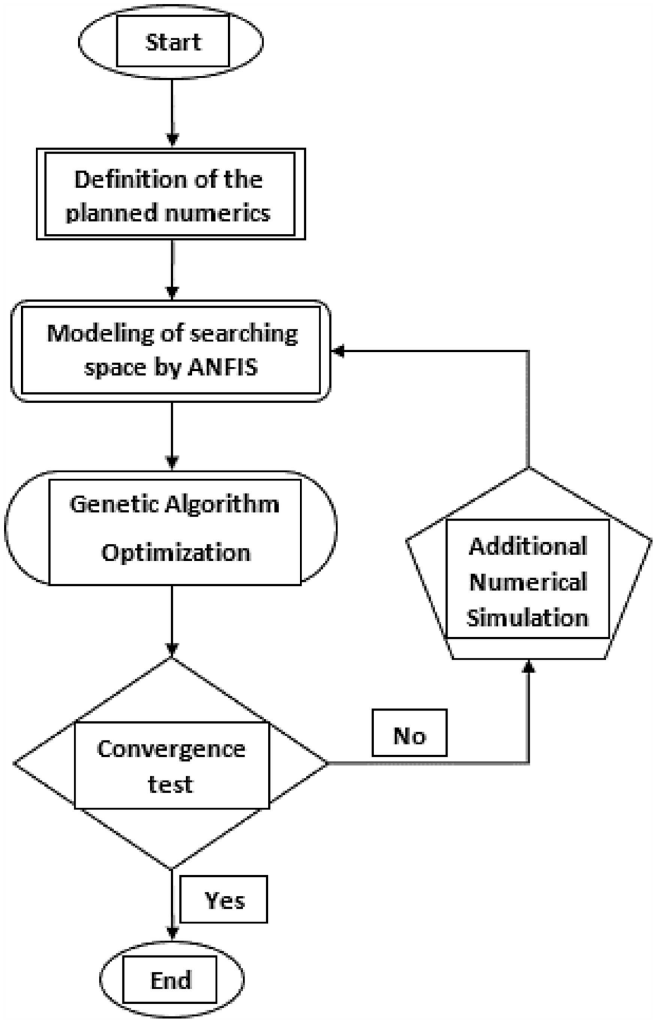

Fig. 6. Optimization process using genetic algorithm.

Sensitivity Analysis

Sensitivity analysis, a technique often applied in financial assessments, was used to calculate the effects of variations in input variables on the target variables. This analysis facilitated projections on the potential outcomes of decisions, grounded in a predefined set of variables. Through the simulation of diverse input variables, experts were enabled to explore the dynamics between changes in a particular variable and the impacted outcomes.

In the study presented, the response surface methodology (RSM) has been used to augment aerodynamic efficiency. The chief objective of this optimization was the determination of optimal values for external factors such as camber ($0 \le Ca \le 0.04$), h/c distance ($0.1 \le h/c \le 0.8$), AOA ($2.5 \le \alpha \le 7.5°$), and thickness ($0.09 \le t \le 0.15$), respectively. The goal was the maximization of the L/D ratio as a measure of aerodynamic performance. The employed RSM model, based on a central composite design (face-centered), was focused on improving L/D as the response variable. The evaluation of the model's efficacy was carried out through an analysis of residual plots. The normality of residuals was confirmed by both a normal probability plot and a histogram. Furthermore, the analysis of variance (ANOVA) table served to evaluate the model's relevance and the significance of its components. The statistical significance of a parameter was established when the p-value fell below 5%, indicating a 95% level of confidence. The F-value, representing the ratio of two variances or mean squares, was used to underline the significance of the findings. Mean squares, being variances adjusted for degrees of freedom (DF), were critical in estimating variance. The statistical analysis conducted affirmed the suitability of the proposed modified Cubic model for L/D in this research.

The study of sensitivity in the design of WIG vehicles is pivotal to the enhancement of their aerodynamic performance and operational efficiency. The introduction of an ANFIS provides a novel methodological approach to navigating the complex objective function for optimization (Djavareshkian and Esmaeili 2013). This allows for a nuanced analysis of how variations in design variables like aerofoil shape, ground clearance, angle of attack, thickness, and camber impact the efficacy of the ground effect. The methodology employed involves the synthesis of GAs and CFD, enabling the precise modeling of aerodynamic forces. This integration facilitates a detailed sensitivity analysis to ascertain the influence of key design parameters on the aerodynamic attributes of WIG vehicles.

According to the aerodynamics theory, camber directly affects the curvature of the aerofoil's mean line (Chang 1970; Gudmundsson 2022). Higher camber typically means more lift because it causes a more significant pressure differential between the pressure and suction sides. This pressure differential is the driving force behind the generation of lift. The effects of camber are prevalent over a wide range of AOA, which makes its influence significant in the overall aerodynamic performance, contributing to a high sensitivity in the overall design (see Fig. 8). Camber has emerged as the preeminent variable, influencing 36% of the sensitivity, marking it as an integral aspect of aerodynamic optimization for WIG vehicles. Fig. 8 indicates that even marginal adjustments in camber can result in considerable changes to the aerodynamic profile, thereby necessitating careful consideration during design and optimization processes. Moreover, in the design of WIG vehicles, where maintaining lift close to the ground is essential, the camber can be optimized to enhance the ground effect, which can significantly improve the L/D ratio at operational altitudes. In the vicinity of the ground, both camber and ground clearance become influential. The camber will continue to play a vital role in generating lift, but the proximity to the ground means that ground clearance also becomes crucial. At these altitudes, the lift is augmented, and drag is reduced because of the ground effect, making ground clearance a highly effective factor in improving L/D.

Fig. 8 highlights the significance of ground clearance, measured as the h/c ratio, for WIG vehicles. The h/c, representing ground clearance, commands a substantial 31% of the total sensitivity. The ground effect, which notably enhances lift while diminishing drag, is accentuated when the wing operates in close proximity to the ground. This near-ground operation modifies airflow patterns around the wing, leading to a decrease in air velocity beneath the wing and consequently, a reduction in lift-induced drag. Given the ground effect's reliance on the wing-to-ground distance, ground clearance emerges as a crucial factor, underscoring its elevated sensitivity and precise modulation of ground clearance is essential given its pronounced effect on the vehicle's aerodynamics.

While AOA is essential for lift generation, its operational range is confined to avoid reaching the critical AOA, beyond which an aircraft stalls. At this juncture, the L/D ratio sharply declines. For WIG vehicles, that predominantly operate in close ground proximity, an optimal AOA range is fundamental to exploit the ground effect fully. Hence, while AOA is crucial, its relative sensitivity (22%) is mitigated when compared with the overriding effects of camber and ground clearance, as depicted in Fig. 8. Consequently, Fig. 8 illustrates that its sensitivity is lower than that of the camber and h/c ratio.

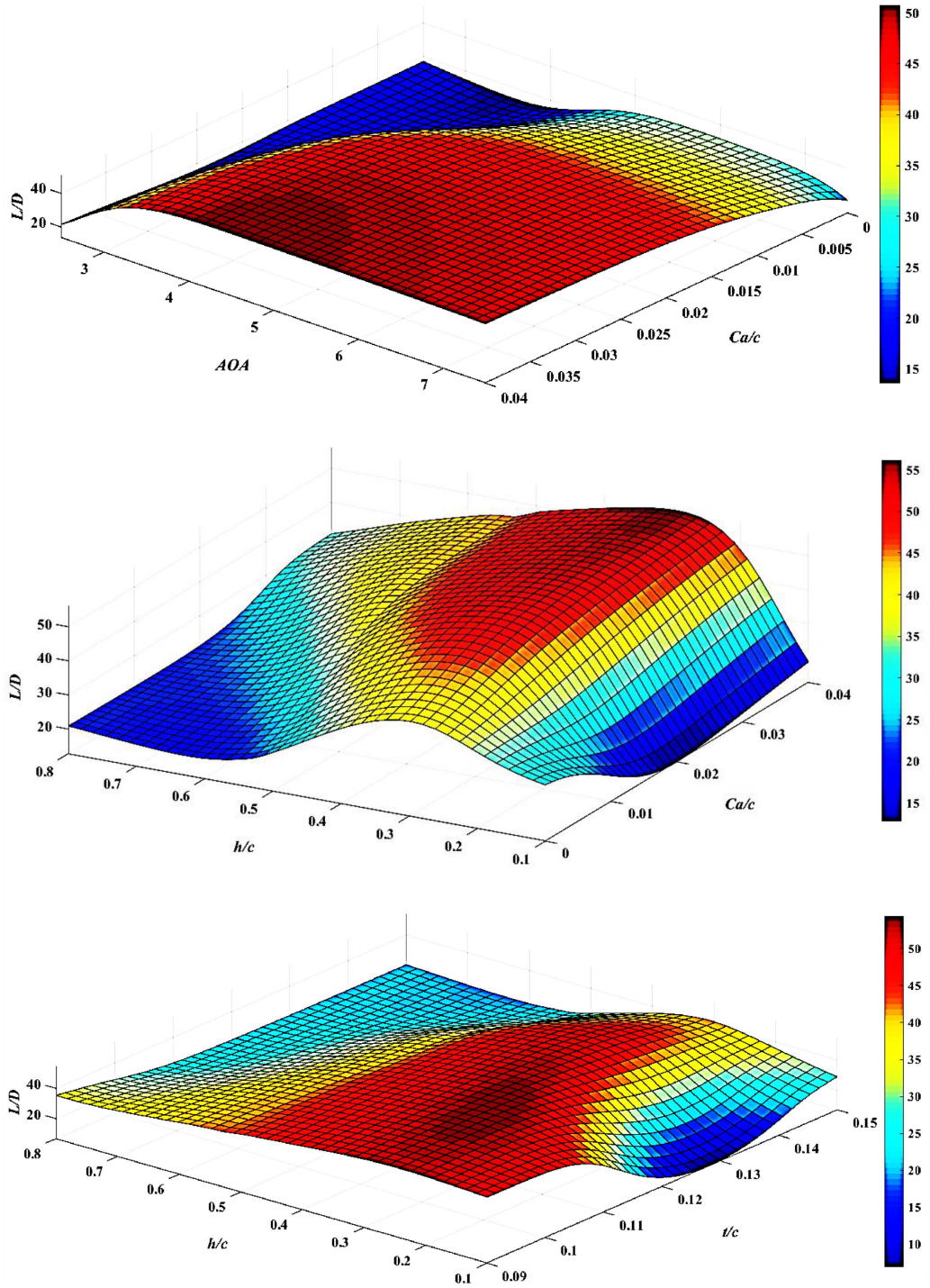

Fig. 7. Approximated search spaces at the 18th optimization level.

The impact of an aerofoil's thickness on its aerodynamic characteristics, such as drag, is acknowledged within the context of aerodynamics theory. However, when considering WIG vehicles, it's important to note that the significance of aerofoil thickness in influencing aerodynamics diminishes compared to factors such as camber and ground clearance (Fig. 8). This is because of the thickness of the aerofoil having been likely optimized to a degree where its effect on aerodynamic performance is less critical. Within the WIG vehicle context, Fig. 8 suggests that while the thickness does affect aerodynamics, its significance (11% sensitivity) is relatively subdued against camber and ground clearance factors. Aerofoil thickness, presumably already fine-tuned for these vehicles, impacts structural robustness and accommodation of internal components more than aerodynamic efficiency per se. Variations in thickness are less likely to significantly alter the L/D ratio, especially in comparison to other more dominant aerodynamic factors.

Camber plays a pivotal role in the aerodynamic optimization of surfaces, exerting the most significant impact on L/D at 36% (Fig. 8). As Fig. 9(a) illustrated, the intricate interplay between AOA, camber, and L/D reveals a complex, possibly nonlinear relationship. These plots not only demonstrate how camber interacts with other aerodynamic parameters but also highlight distinct regions where

J. Aerosp. Eng., 2026, 39(1): 04025118

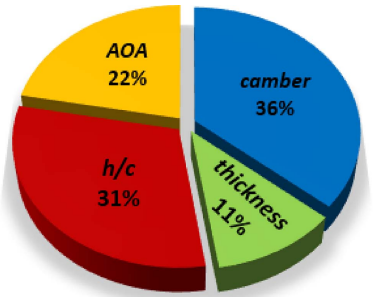

Fig. 8. The proportion of camber, thickness, AOA and h/c based on sensitivity analysis.

L/D is notably improved. There appears to be an optimal AOA range that maximizes the L/D ratio, likely marking the threshold for optimal lift generation before the adverse effects of stall set in. Similarly, the camber's influence on L/D exhibits a nonlinear behavior, with an ideal camber value that optimizes L/D within a specific AOA range.

The sensitivity of L/D to variations in AOA and camber is clearly depicted through the curvature observed in the surface plots, indicating that achieving peak aerodynamic performance requires precise tuning of these parameters. The relationship between AOA and aerodynamic efficiency is nonlinear; performance enhancements are evident up to a certain AOA threshold, beyond which the benefits either plateau or diminish, suggesting a parabolic relationship.

Aerodynamic efficiency is fundamentally influenced by two critical parameters: the thickness and camber of an aerofoil. An inverse relationship, potentially linear as depicted in Fig. 9(b), exists between the aerofoil's thickness and its aerodynamic efficiency. Specifically, increased thickness tends to elevate drag, diminishing efficiency. On the other hand, the interplay between camber and aerodynamic performance is distinctly nonlinear and positive, indicating the presence of an optimal camber that enhances lift forces without significantly boosting drag. However, exceeding this optimal camber threshold can lead to a detrimental surge in drag. The synergy among aerofoil thickness, camber, and the L/D ratio is complex and likely nonlinear. The impact of aerofoil thickness on the boundary layer characteristics, and consequently on drag, is significant. There exists an optimal combination of thickness and camber that achieves the maximum L/D ratio. This optimal balance leverages the lift enhancement provided by camber while mitigating the parasitic and induced drag introduced by thickness. The graphical representation identifies a peak in the L/D ratio within this optimal zone. Advancements beyond this peak, either through increased thickness or deviation from the optimal camber, result in a decline in the L/D ratio, attributed to an excessive rise in drag.

Fig. 9(c) illustrates how the aerodynamic performance of a vehicle is significantly influenced by its ground clearance, which demonstrates a complex, nonlinear relationship with aerodynamics. Ground clearance reaches a critical threshold where the ground effect is maximized, thereby optimizing aerodynamic performance. This intricate balance highlights the challenges in achieving an ideal aerodynamic design, necessitating a harmonious adjustment of various parameters, including camber, AOA, thickness, and ground clearance, to enhance overall efficiency. The interplay between h/c, camber, and L/D ratio is particularly nuanced, reflecting the intricate dynamics of the ground effect. As the h/c ratio decreases, indicating a reduction in ground clearance, the L/D ratio experiences an upturn because of an increase in lift and a decrease in induced drag. This trend continues until reaching a point where exceedingly close proximity to the ground introduces adverse flow patterns, potentially indicated by a decline in the surface plot. The adjustment of camber emerges as a pivotal factor in this context, with an optimally designed camber capable of exploiting the ground effect to its fullest advantage. This optimal exploitation is evidenced by the peak regions on the plot, emphasizing the critical role of camber in modulating ground effect to achieve peak aerodynamic performance.

In Fig. 9(d), which examines the relationship between AOA, h/c, and L/D, it was observed that the L/D ratio varies with changes in AOA and h/c. With the increase in AOA to a certain degree, the L/D ratio is enhanced, indicating a rise in lift that outpaces the increase in drag. Concurrently, as the h/c ratio diminishes, signifying closer proximity to the ground, the L/D ratio improves because of the ground effect, which boosts lift and reduces drag. However, a further decrease in h/c beyond a critical point inversely affects the L/D ratio, possibly because of unfavorable aerodynamic interactions at extremely low ground clearances (Jabbari et al. 2021).

Fig. 9(e) focuses on the interaction between h/c, thickness, and L/D. Here, a nonlinear relationship is evident. A moderate increase in thickness leads to a higher L/D ratio, likely because of the improved lift from the enhanced aerofoil curvature. Nonetheless, the plot suggests that excessive thickness incurs a disproportionate increase in drag, which overwhelms the lift benefits, reducing the L/D ratio. The ground effect, modulated by h/c, exhibits an optimal zone where the L/D ratio is at its peak, reinforcing the significance of balanced design parameters.

Fig. 9(f) depicts the relationship between thickness, AOA, and L/D. This surface plot shows that increasing the thickness while maintaining a low AOA appears to degrade the L/D ratio, likely because of increased drag that is not compensated by lift. In contrast, at higher AOAs, the L/D ratio improves with an increase in thickness up to a threshold, beyond which the benefits of added lift are negated by the corresponding increase in drag.

The sensitivity analysis within the RSM optimization framework, specifically in the context of central composite design (CCD), outlines the proposed relationships between the L/D ratio and various geometric parameters. These relationships are presented in Eq. (13) as

$$\begin{aligned} \boldsymbol{L/D} = {} & 10^3 \times (0.8729 - (1.1820 \times Ca) - (20.2717 \times t) + (0.1439 \times h/c) - (0.05503 \times AOA) + (50.4517 \times Ca \times t) \\ & - (0.4694 \times Ca \times h/c) - (0.02952 \times Ca \times AOA) + (0.04371 \times t \times h/c) + (0.02889 \times t \times AOA) + (0.000376 \times h/c \times AOA) \\ & - (43.8312 \times Ca^2) + (170.372 \times t^2) - (0.40621 \times h/c^2) + (0.01198 \times AOA^2) + (2105.67 \times Ca^2 \times t) \\ & + (19.7214 \times Ca^2 \times h/c) - (0.001849 \times Ca \times t^2) - (0.004712 \times t^3) + (0.2899 \times h/c^3) - (0.000837 \times AOA^3) \\ & - (4800.61 \times Ca \times t^3) - (3.7827 \times t^3 \times h/c) \end{aligned} \tag{13}$$

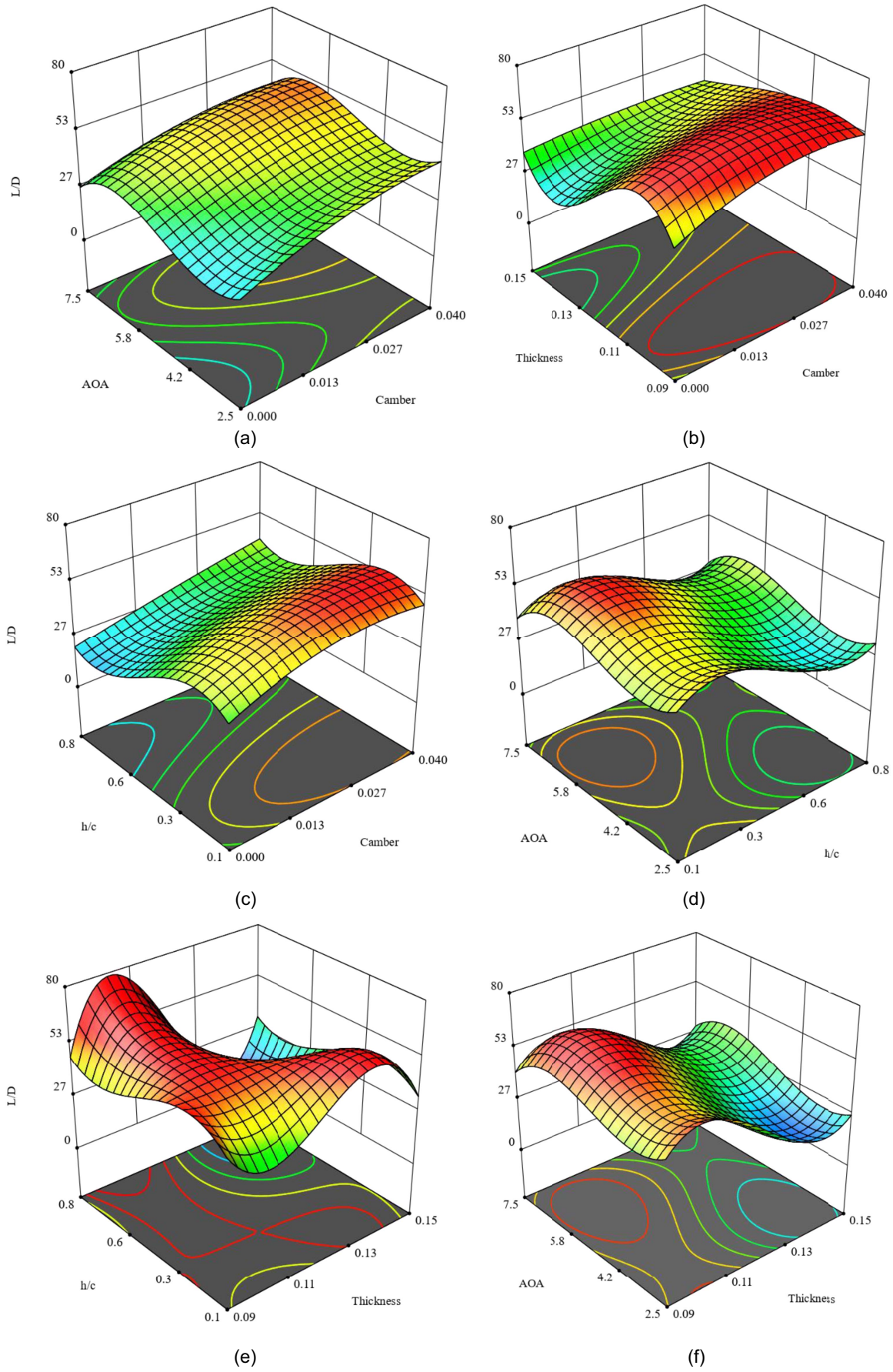

Fig. 9. Response surface visualization for four factors of (a) AOA-camber; (b) thickness-camber; (c) h/c-camber; (d) AOA-h/c; (e) h/c-thickness; and (f) AOA-thickness to study the interactive impacts.

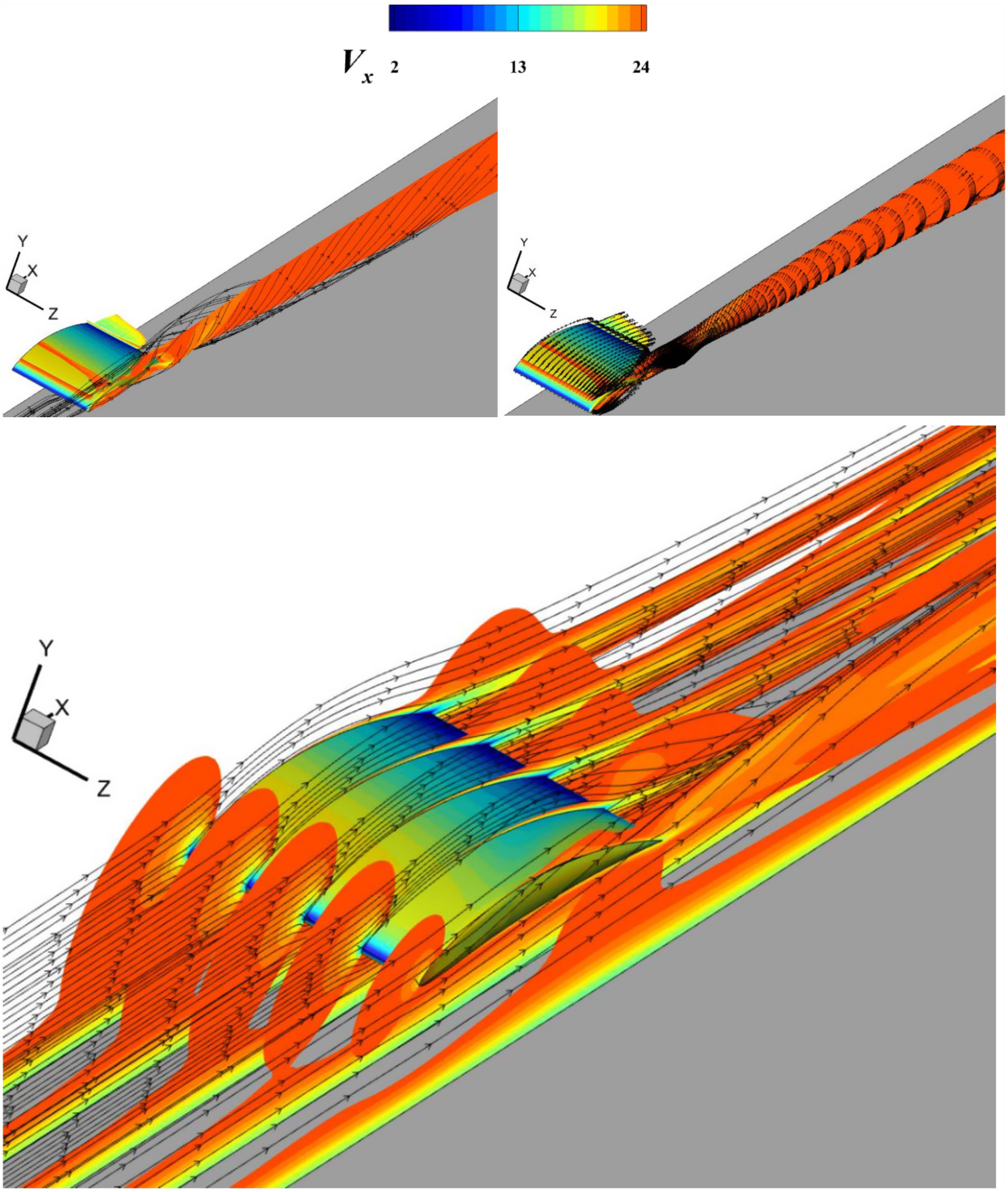

Fig. 10. Velocity contour around the optimized wing in the vicinity of the ground.

Collectively, these results underscore the complexity of the design space for WIG vehicles. The sensitivity analysis carried out using ANFIS aids in discerning the intricate balance necessary to optimize the aerodynamic shape, considering the multifaceted interaction between design variables and their impact on aerodynamic efficiency. The careful calibration of camber, h/c, AOA, and thickness is essential to harness the ground effect and achieve superior L/D ratios, which are indicative of enhanced aerodynamic performance and operational efficiency. This analysis is instrumental in guiding the design and optimization of WIG vehicles, contributing significantly to the field of computational aerodynamics.

In-Depth Evaluation of Flow Characteristics

Fig. 10 illustrates how the velocity contours reveal the x-velocity variation across multiple streamwise sections of the wing, as defined by the specifications in Table 7. These specifications include $AR = 1$, a camber of 3.99%, a thickness of 12.17%, an h/c ratio of approximately 0.21, and an angle of attack just over 6.68 degrees.

According to aerodynamics theory, the distribution of velocity around an aerofoil is fundamental to the generation of aerodynamic forces (Gad-el-Hak 1990; Li et al. 2016; Liu 2021; Wu et al. 2018). The velocity contours reveal higher velocities on the wing's suction side, indicating lower pressure, and lower velocities on the pressure side, indicating higher pressure. This differential in pressure is crucial for lift generation. The pattern of airflow, as depicted by the contour lines, mirrors changes in airspeed over the wing's surface. The smooth transition in gradients and the absence of sudden shifts in the contours suggest that the airflow remains attached to the wing's surface. This attachment is essential for sustaining stable lift and preventing stall conditions. To build upon the claim during sensitivity analysis, camber optimization emerges as a critical factor through the analysis of velocity contours. Variations in the contours' gradients along the camber line indicate that slight adjustments in camber can significantly affect local velocities, thereby influencing lift. This observation underscores the camber's high sensitivity in relation to overall aerodynamic performance.

Furthermore, the contours highlight the impact of ground effect on velocity distribution, particularly near the wing's trailing edge and lower surface. This effect illustrates the wing's interaction with ground proximity, supporting the assigned sensitivity of 31% to ground clearance. Near the ground, the velocity contours alter, demonstrating the ground effect's role in enhancing lift and reducing drag. This compression of airflow beneath the wing is evidenced by denser contour lines on the lower surface, signifying increased velocities that contribute to a decrease in lift-induced drag. The significant influence of camber and ground clearance on velocity distribution corroborates their sensitivity percentages (36% and 31%, respectively). The contours' relative uniformity in the direction of thickness suggests optimal status, supporting the assigned lower sensitivity percentage (11%).

Conclusions

This study represents a significant advancement in the aerodynamic optimization of WIG vehicles, offering both a comprehensive analysis and an innovative framework that bridges the gap between theoretical research and real-world applications. By systematically examining the effects of camber, thickness, AOA, and h/c on aerodynamic performance, the research has provided valuable insights into how these parameters influence the L/D. Notably, the sensitivity analysis revealed that camber is the most influential parameter, accounting for a 36% variation in aerodynamic efficiency, followed by h/c with a 31% impact. Although the angle of attack and thickness also contribute significantly, with sensitivities of 22% and 11% respectively, their impact is less pronounced compared to camber and ground clearance.

The application of GA in conjunction with CFD simulations has enabled the optimization of these key design parameters, leading to a remarkable improvement in the L/D ratio by up to 55.89%. This enhancement highlights the critical role of these design parameters in improving fuel efficiency and extending the operational range of WIG vehicles. Such improvements are not only crucial for the performance of these vehicles but also have the potential to reduce the environmental footprint of aerial transportation, marking a significant step toward more sustainable aviation solutions. Furthermore, the integration of the ANFIS with GA and CFD simulations has proven to be a powerful methodological innovation. This combination offers a more nuanced understanding of the complex interplay between aerodynamic variables, allowing for the precise modeling of aerodynamic forces. The approach employed in this study provides a robust platform for the future design of high-performance, environmentally friendly WIG vehicles. By modeling the aerodynamic forces with greater accuracy, this research lays the groundwork for developing vehicles that are not only efficient but also capable of operating in harmony with the environment.

This study sets a new standard for the aerodynamic design and optimization of WIG vehicles, contributing to the broader field of computational aerodynamics and optimization. The findings offer a solid foundation for future research aimed at further enhancing the design of efficient, sustainable aerial transportation systems, pushing the boundaries of what is achievable in the quest for greener, more efficient flight technologies. The methodologies developed here are applicable beyond WIG vehicles, providing valuable insights for other aerodynamics industries seeking to optimize performance through computational optimization techniques.

Data Availability Statement

Some or all data, models, or code that support the findings of this study are available from the corresponding author upon reasonable request.

Acknowledgments

This research was funded by Ferdowsi University of Mashhad (Grant No. 2/55864). The financial support is gratefully acknowledged.

Author Contributions

Hossein Jabbari: Conceptualization; Data curation; Formal analysis; Investigation; Methodology; Project administration; Resources; Software; Validation; Visualization; Writing – original draft; Writing – review and editing. Ali Esmaeili: Conceptualization; Data curation; Formal analysis; Investigation; Methodology; Project administration; Resources; Software; Supervision; Validation; Visualization; Writing – original draft; Writing – review and editing.

References

Abu Salem, K., G. Palaia, M. R. Chiarelli, and M. Bianchi. 2023. "A simulation framework for aircraft take-off considering ground effect aerodynamics in conceptual 7 design." *Aerospace* 10 (5): 459. https://doi.org/10.3390/aerospace10050459.

Ahmed, M. R., and S. D. Sharma. 2005. "An investigation on the aerodynamics of a symmetrical airfoil in ground effect." *Exp. Therm. Fluid Sci.* 29 (6): 633–647. https://doi.org/10.1016/j.expthermflusci.2004.09.001.

Ahmed, M. R., T. Takasaki, and Y. Kohama. 2007. "Aerodynamics of a NACA4412 airfoil in ground effect." *AIAA J.* 45 (1): 37–47. https://doi.org/10.2514/1.23872.

Aly, S., M. Ogot, and R. Peltz. 1996. "Stochastic approach to optimal aerodynamic shape design." *J. Aircr.* 33 (5): 956–961. https://doi.org/10.2514/3.47041.

Anderson, W. K., and D. L. Bonhaus. 1999. "Airfoil design on unstructured grids for turbulent flows." *AIAA J.* 37 (2): 185–191. https://doi.org/10.2514/2.712.

Angrand, F. 1983. "Optimum design for potential flows." *Int. J. Numer. Methods Fluids* 3 (3): 265–282. https://doi.org/10.1002/fld.1650030306.

Arnaldo Valdés, R. M., S. Burmaoglu, V. Tucci, L. M. Braga da Costa Campos, L. Mattera, and V. F. Gomez Comendador. 2019. "Flight path 2050 and ACARE goals for maintaining and extending industrial

leadership in aviation: A map of the aviation technology space." *Sustainability* 11 (7): 2065. https://doi.org/10.3390/su11072065.
Chang, P. K. 1970. "Control of separation of flow." In *Separation of flow*, 716–752. Amsterdam, Netherlands: Elsevier. https://doi.org/10.1016/B978-0-08-013441-3.50016-2.
Chernukhin, O., and D. W. Zingg. 2013. "Multimodality and global optimization in aerodynamic design." *AIAA J.* 51 (6): 1342–1354. https://doi.org/10.2514/1.J051835.
Conlan-Smith, C., N. Ramos-García, and C. Schousboe Andreasen. 2022. "Aerodynamic shape optimization of highly nonplanar raised and drooped wings." *J. Aircr.* 59 (1): 206–218. https://doi.org/10.2514/1.C036403.
Conlan-Smith, C., N. Ramos-García, O. Sigmund, and C. S. Andreasen. 2020. "Aerodynamic shape optimization of aircraft wings using panel methods." *AIAA J.* 58 (9): 3765–3776. https://doi.org/10.2514/1.J058979.
Djavareshkian, M. H., and A. Esmaeili. 2013. "Neuro-fuzzy based approach for estimation of hydrofoil performance." *Ocean Eng.* 59 (Feb): 1–8. https://doi.org/10.1016/j.oceaneng.2012.10.015.
Djavareshkian, M. H., A. Esmaeli, and A. Parsani. 2011. "Aerodynamics of smart flap under ground effect." *Aerosp. Sci. Technol.* 15 (8): 642–652. https://doi.org/10.1016/j.ast.2011.01.005.
Elliott, J., and J. Peraire. 1997. "Practical three-dimensional aerodynamic design and optimization using unstructured meshes." *AIAA J.* 35 (9): 1479–1485. https://doi.org/10.2514/2.271.
Fevralskikh, A. 2022. "A development of longitudinal static stability analysis method of a wing-in-ground effect vehicle in cruise during the design process." *Ocean Eng.* 243 (Jan): 110187. https://doi.org/10.1016/j.oceaneng.2021.110187.
Foshat, S. 2020. "Numerical investigation of the effects of plasma actuator on separated laminar flows past an incident plate under ground effect." *Aerosp. Sci. Technol.* 98: 105646. https://doi.org/10.1016/j.ast.2019.105646.
Gad-el-Hak, M. 1990. "Control of low-speed airfoil aerodynamics." *AIAA J.* 28 (9): 1537–1552. https://doi.org/10.2514/3.25250.
Gagnon, H., and D. W. Zingg. 2016. "Euler-equation-based drag minimization of unconventional aircraft configurations." *J. Aircr.* 53 (5): 1361–1371. https://doi.org/10.2514/1.C033591.
Gudmundsson, S. 2022. "The anatomy of the airfoil." In *General aviation aircraft design*, 257–319. Amsterdam, Netherlands: Elsevier. https://doi.org/10.1016/B978-0-12-818465-3.00008-2.
Hasan, M., S. Redonnet, and D. Zhongmin. 2025. "Aerodynamic optimization of aircraft wings using machine learning." *Adv. Eng. Software* 200 (Feb): 103801. https://doi.org/10.1016/j.advengsoft.2024.103801.
Hu, H., G. Zhang, D. Li, Z. Zhang, T. Sun, and Z. Zong. 2022. "Shape optimization of airfoil in ground effect based on free-form deformation utilizing sensitivity analysis and surrogate model of artificial neural network." *Ocean Eng.* 257 (Aug): 111514. https://doi.org/10.1016/j.oceaneng.2022.111514.
Jabbari, H., A. Esmaeili, and S. Rabizadeh. 2021. "Phase portrait analysis of laminar separation bubble and ground clearance interaction at critical (low) Reynolds number flow." *Ocean Eng.* 238 (Oct): 109731. https://doi.org/10.1016/j.oceaneng.2021.109731.
Jameson, A. 1988. "Aerodynamic design via control theory." *J. Sci. Comput.* 3 (3): 233–260. https://doi.org/10.1007/BF01061285.
Jameson, A., and J. Reuther. 1994. "Control theory based airfoil design using the Euler equations." In *Proc., 5th Symp. on Multidisciplinary Analysis and Optimization*, 4274. Reston, VA: American Institute of Aeronautics and Astronautics. https://doi.org/10.2514/6.1994-4272.
Jang, J. S. R., C. T. Sun, and E. Mizutani. 1997. "Neuro-fuzzy and soft computing—A computational approach to learning and machine intelligence." *IEEE Trans. Autom. Control* 42 (10): 1482–1484. https://doi.org/10.1109/TAC.1997.633847.
Jansen, P. W., R. E. Perez, and J. R. R. A. Martins. 2010. "Aerostructural optimization of nonplanar lifting surfaces." *J. Aircr.* 47 (5): 1490–1503. https://doi.org/10.2514/1.44727.
Jesudasan, R., A. Hanifi, and R. Mariani. 2023. "Investigating planar and nonplanar wing planform optimisation for ground effect aircraft." *Aerospace* 10 (11): 969. https://doi.org/10.3390/aerospace10110969.
Koo, D., and D. W. Zingg. 2018. "Investigation into aerodynamic shape optimization of planar and nonplanar wings." *AIAA J.* 56 (1): 250–263. https://doi.org/10.2514/1.J055978.
Lee, S.-H., and J. Lee. 2013. "Aerodynamic analysis and multi-objective optimization of wings in ground effect." *Ocean Eng.* 68 (Aug): 1–13. https://doi.org/10.1016/j.oceaneng.2013.04.018.
Li, J., X. Du, and J. R. R. A. Martins. 2022. "Machine learning in aerodynamic shape optimization." *Prog. Aerosp. Sci.* 134 (Oct): 100849. https://doi.org/10.1016/j.paerosci.2022.100849.
Li, Q., T. Maeda, Y. Kamada, J. Murata, K. Furukawa, and M. Yamamoto. 2016. "The influence of flow field and aerodynamic forces on a straight-bladed vertical axis wind turbine." *Energy* 111 (Sep): 260–271. https://doi.org/10.1016/j.energy.2016.05.129.
Li, Z., C. Lan, L. Jia, and Y. Ma. 2017. "Ground effects on separated laminar flows past an inclined flat plate." *Theor. Comput. Fluid Dyn.* 31 (2): 127–136. https://doi.org/10.1007/s00162-016-0410-0.
Liu, T. 2021. "Evolutionary understanding of airfoil lift." *Adv. Aerodyn.* 3 (1): 37. https://doi.org/10.1186/s42774-021-00089-4.
Lou, J., R. Chen, J. Liu, Y. Bao, Y. You, and Z. Chen. 2023. "Aerodynamic optimization of airfoil based on deep reinforcement learning." *Phys. Fluids* 35 (3): 037128. https://doi.org/10.1063/5.0137002.
Lyu, Z., and J. R. R. A. Martins. 2014. "Aerodynamic design optimization studies of a blended-wing-body aircraft." *J. Aircr.* 51 (5): 1604–1617. https://doi.org/10.2514/1.C032491.
Morris, A. M., C. B. Allen, and T. C. S. Rendall. 2009. "Aerodynamic shape optimization of a modern transport wing using only planform variations." *Proc. Inst. Mech. Eng., Part G: J. Aerosp. Eng.* 223 (6): 843–851. https://doi.org/10.1243/09544100JAERO393.
Nemec, M., D. W. Zingg, and T. H. Pulliam. 2004. "Multipoint and multi-objective aerodynamic shape optimization." *AIAA J.* 42 (6): 1057–1065. https://doi.org/10.2514/1.10415.
Nielsen, E. J., and W. K. Anderson. 1999. "Aerodynamic design optimization on unstructured meshes using the Navier-Stokes equations." *AIAA J.* 37 (11): 1411–1419. https://doi.org/10.2514/2.640.
Ning, S. A., and I. Kroo. 2010. "Multidisciplinary considerations in the design of wings and wing tip devices." *J. Aircr.* 47 (2): 534–543. https://doi.org/10.2514/1.41833.
Park, K., and J. Lee. 2010. "Optimal design of two-dimensional wings in ground effect using multi-objective genetic algorithm." *Ocean Eng.* 37 (10): 902–912. https://doi.org/10.1016/j.oceaneng.2010.03.001.
Pironneau, O. 1974. "On optimum design in fluid mechanics." *J. Fluid Mech.* 64 (1): 97–110. https://doi.org/10.1017/S0022112074002023.
Reist, T. A., and D. W. Zingg. 2017. "High-fidelity aerodynamic shape optimization of a lifting-fuselage concept for regional aircraft." *J. Aircr.* 54 (3): 1085–1097. https://doi.org/10.2514/1.C033798.
Simanowitsch, D., A. Sudhi, A. Theiss, C. Badrya, and S. Hein. 2022. "Comparison of gradient-based and genetic algorithms for laminar airfoil shape optimization." In *Proc., AIAA SCITECH 2022 Forum*. San Diego: American Institute of Aeronautics and Astronautics. https://doi.org/10.2514/6.2022-0008.
Teimourian, A., D. Rohacs, K. Dimililer, H. Teimourian, M. Yildiz, and U. Kale. 2024. "Airfoil aerodynamic performance prediction using machine learning and surrogate modeling." *Heliyon* 10 (8): e29377–e29377. https://doi.org/10.1016/j.heliyon.2024.e29377.
Wu, J., L. Liu, and T. Liu. 2018. "Fundamental theories of aerodynamic force in viscous and compressible complex flows." *Prog. Aerosp. Sci.* 99 (May): 27–63. https://doi.org/10.1016/j.paerosci.2018.04.002.
Xu, M., S. Song, X. Sun, W. Chen, and W. Zhang. 2021. "Machine learning for adjoint vector in aerodynamic shape optimization." *Acta Mech. Sin.* 37 (9): 1416–1432. https://doi.org/10.1007/s10409-021-01119-6.
Yun, L., A. Bliault, and J. Doo. 2010. *WIG craft and ekranoplan*. Berlin: Springer. https://doi.org/10.1007/978-1-4419-0042-5.
Zhang, X., and J. Zerihan. 2003. "Aerodynamics of a double-element wing in ground effect." *AIAA J.* 41 (6): 1007–1016. https://doi.org/10.2514/2.2057.
Zingg, D. W., M. Nemec, and T. H. Pulliam. 2008. "A comparative evaluation of genetic and gradient-based algorithms applied to aerodynamic optimization." *Eur. J. Comput. Mech.* 17 (1–2): 103–126. https://doi.org/10.3166/remn.17.103-126.